8006 *Biochemistry* **2010,** *49,* 8006–8019
DOI: 10.1021/bi100508u

BIOCHEMISTRY
including biophysical chemistry & molecular biology
Article

Backbone Amide Dynamics Studies of Apo-L75F-TrpR, a Temperature-Sensitive Mutant of the Tryptophan Repressor Protein (TrpR): Comparison with the ^{15}N NMR Relaxation Profiles of Wild-Type and A77V Mutant Apo-TrpR Repressors[†]

Anupam Goel,[‡] Brian P. Tripet,[‡] Robert C. Tyler,[‡,§] Lucas D. Nebert,[‡] and Valérie Copié*[,‡]

[‡]*Department of Chemistry and Biochemistry, Montana State University, Bozeman, Montana 59717, and*
[§]*Department of Biochemistry, Medical College of Wisconsin, Milwaukee, Wisconsin 53226*

Received April 4, 2010; Revised Manuscript Received August 16, 2010

ABSTRACT: Backbone amide dynamics studies were conducted on a temperature-sensitive mutant (L75F-TrpR) of the tryptophan repressor protein (TrpR) of *Escherichia coli* in its apo (i.e., no L-tryptophan corepressor-bound) form. The ^{15}N NMR relaxation profiles of apo-L75F-TrpR were analyzed and compared to those of wild-type (WT) and super-repressor mutant (A77V) TrpR proteins, also in their apo forms. The ^{15}N NMR relaxation data (^{15}N-T_1, ^{15}N-T_2, and heteronuclear ^{15}N−{^{1}H}-nOe) recorded on all three aporepressors at a magnetic field strength of 600 MHz (^{1}H Larmor frequency) were analyzed to extract dynamics parameters, including diffusion tensor ratios ($D_\parallel/D_\perp$), correlation times (τ_m) for overall reorientations of the proteins in solution, reduced spectral density terms [$J_{eff}(0)$, $J(0.87\omega_H)$, $J(\omega_N)$], and generalized order parameters (S^2), which report on protein internal motions on the picosecond to nanosecond and slower microsecond to millisecond chemical exchange time scales. Our results indicate that all three aporepressors exhibit comparable $D_\parallel/D_\perp$ ratios and characteristic time constants, τ_m, for overall global reorientation, indicating that in solution, all three apoproteins display very similar overall shape, structure, and rotational diffusion properties. Comparison of ^{15}N NMR relaxation data, reduced spectral density profiles, and generalized S^2 order parameters indicated that these parameters are quite uniform for backbone amides positioned within the four (A−C and F) core α-helices of all three aporepressors. In contrast, small but noticeable differences in internal dynamics were observed for backbone amides located within the helix D−turn−helix E DNA-binding domain of the apo-TrpR proteins. The significance of these dynamics differences in terms of the biophysical characteristics and ligand binding properties of the three apo-TrpR proteins is discussed.

The tryptophan repressor protein (TrpR)[1] from *Escherichia coli* is a 25 kDa homodimeric protein comprised of two identical 108-residue polypeptide chains (*1*). TrpR regulates the biosynthesis of L-Trp, and its mode of function is considered to be a paradigm of transcriptional and allosteric regulation (*2*). In the absence of L-Trp, the aporepressor displays a low affinity for DNA. When two L-Trp molecules bind per dimer, TrpR's binding affinity for operator-specific DNA of several operons responsible for the uptake and biosynthesis of L-tryptophan and other biological molecules is enhanced significantly (*3*−*6*). The operons regulated by TrpR include *trpEDCBA*, *trpR*, *aroH*, and *mtr* (*3*−*6*).

TrpR regulates transcription of distinct genes in these operons by binding to their DNA operator regions whose sequences share nucleotide similarities but are not identical. Thus, one of the requirements for proper TrpR function is that the repressor be able to bind DNA with high affinity in response to cellular metabolic needs and to interact specifically with specific DNA operator sequences to ensure proper selection of the DNA operon(s) whose transcription must be regulated. A key to TrpR function thus involves biophysical characteristics that permit the modulation of the repressor's binding affinity for DNA, specificity, and stoichiometry (i.e., number of repressor dimer molecules bound per DNA equivalents) (*7*, *8*).

For TrpR, these properties are modulated by the binding of the L-Trp corepressor, which acts as an allosteric effector altering the repressor's affinity for DNA via the protein's L-Trp cofactor binding sites (*1*, *8*−*10*). Studies have demonstrated that L-Trp binding modulates TrpR repressor specificity and not solely affinity, and that both the L-Trp corepressor and the cognate DNA operator function together to achieve repressor activation. The unique characteristics of TrpR arise in part from the intertwined structure of its two protomers in the TrpR dimer, and the extensive flexibility of its structure (*11*).

Extensive structural studies by both X-ray (*12*−*14*) and NMR (*15*, *16*) have shown that TrpR is comprised of six α-helices per monomer, helices A−F. Helices A−C and F of the two protomers come together to form the hydrophobic core of the TrpR

[†]This work has been supported by National Science Foundation Grant MCB-0444056.

*To whom correspondence should be addressed: Department of Chemistry and Biochemistry, Montana State University, P.O. Box 173400, Bozeman, MT 59717. E-mail: vcopie@chemistry.montana.edu. Phone: (406) 994-7244. Fax: (406) 994-5407.

[1]Abbreviations: CPMG, Carr−Purcell−Meiboom−Gill multipulse sequence; CSA, chemical shift anisotropy; DIPSI, decoupling in the presence of scalar interactions; HSQC, heteronuclear single-quantum coherence spectroscopy; HTH, helix−turn−helix motif; IPTG, isopropyl β-thiogalactoside; 5-MT, 5-methyltryptophan; L-Trp, L-tryptophan; NMR, nuclear magnetic resonance; nOe, nuclear Overhauser effect; TrpR, tryptophan repressor; apo-WT-TrpR, wild-type apo-TrpR repressor; apo-L75F-TrpR, L75F mutant apo-TrpR repressor; A77V-TrpR, A77V mutant apo-TrpR repressor; ts, temperature-sensitive; WALTZ, wideband alternative-phase low-power technique for zero residual splitting.

 Published on Web 08/18/2010

dimer, while helices D and E comprise the helix−turn−helix (HTH) DNA-binding domain of TrpR. Solution structures of apo-WT-TrpR have shown that the repressor's HTH DNA-binding domain is more disordered in solution than in the crystalline state (*15*, *16*). DNA binding upon activation of TrpR by L-Trp binding is thought to take place via a sequential ordering of the protein's helix D−turn−helix E DNA-binding domain, where initially helix E (the recognition helix) becomes more ordered upon formation of the L-Trp-bound holo-TrpR repressor, followed by ordering of helix D upon binding of holo-TrpR to DNA (*16*−*21*). TrpR thus represents an interesting system for structural biology as this protein is extremely thermostable (T_m of ~90 °C with a free energy of folding of 23 kcal/mol per dimer) (*22*, *23*) yet possesses a highly dynamic structure whose flexibility seems to be essential for function (*17*−*20*, *24*, *25*).

Mutagenesis experiments have shown that the flexibility and sequential structural ordering of the HTH DNA-binding domain of TrpR are affected by slight changes in amino acid composition. Such slight changes in primary sequence lead to significant alterations in the L-Trp and DNA binding properties and biological function of the repressor (*26*, *27*). Several TrpR mutants have been classified as "super-repressors" because of their ability to repress gene transcription at lower L-Trp concentrations relative to those needed for proper functioning of WT-TrpR (*28*). For example, the super-repressor TrpR variant, A77V-TrpR, in which alanine 77 is replaced with valine, exhibits a 10% increase in apparent α-helicity as measured by CD, is slightly more stable to urea denaturation, and seems to be less flexible than apo-WT-TrpR (*24*, *29*). DNA-binding studies, interestingly, have also shown that the A77V-TrpR variant cannot recognize the full complement of operator sequences normally accessible to WT-TrpR (*25*). The reduced flexibility of A77V-TrpR is thus thought to be responsible for the restricted specificity of this TrpR mutant to a subset of DNA sequences (*24*). These data support the notion that the dynamics features of the helix D−turn−helix E (HTH) DNA-binding domain of TrpR are a critical source of adaptability. However, despite extensive biochemical and biophysical studies of TrpR and TrpR mutants, the precise mechanisms by which altered flexibility leads to altered TrpR function remain poorly understood.

Because of the potential of temperature-sensitive (ts) mutants to yield additional insights into the interplay among protein structure, dynamics, and function, a genetic screen for potential ts TrpR mutant(s) was undertaken and resulted in the isolation of a TrpR variant, apo-L75F-TrpR, in which leucine 75 is replaced with phenylalanine (*30*). $TrpR^-$ *E. coli* cells transfected with a plasmid encoding L75F-TrpR were able to grow in the presence of 5-methyltryptophan (5-MT) at 42 °C but displayed a significantly reduced level of growth at 37 °C (*30*) (termed the "permissive" and "nonpermissive" temperatures, respectively). 5-MT, an analogue of L-Trp, binds to apo-TrpR ~2 times more tightly (*9*). This results in a 5-MT−TrpR pseudorepressor that binds to operator DNA ~10 times more tightly than holo-TrpR (*31*, *32*). Because 5-MT cannot substitute for the amino acid L-tryptophan during protein synthesis, *E. coli* cells transfected with a functional TrpR starve for L-Trp when grown on minimal medium containing 5-MT instead of L-Trp. In contrast, *E. coli* cells expressing a TrpR variant with an amino acid substitution that alters TrpR function can survive when grown on minimal medium containing 5-MT because the *trpR* operon that controls L-Trp biosynthesis is derepressed and permits production of L-Trp necessary for cell growth (*30*, *33*). The ts screen that resulted in the isolation of L75F-TrpR indicated that this TrpR mutant is a more effective repressor at 37 °C than at 42 °C (*30*).

Biophysical studies have shown that L75F-TrpR is characterized by an ~12% increase in apparent α-helicity, a slightly higher urea denaturation midpoint, and a thermal stability identical to that of WT-TrpR (*30*). Fluorescence and ^1H NMR data also presented early evidence that the Leu to Phe substitution at position 75 produces biochemical perturbations at sites distant from the mutation (*30*). In contrast to the A77V super-repressor TrpR mutant, L75F-TrpR was found to bind the L-Trp corepressor with an ~10 times lower affinity compared to WT-TrpR, and in the presence of excess L-Trp in vitro, holo-L75F-TrpR's affinity for operator DNA was measured to be 2−5 times weaker (*30*). Thus, the L75F mutation was shown to affect not only the biophysical properties of TrpR but also its ligand binding function. However, a detailed molecular mechanism by which a single-point amino acid replacement of a residue located on a solvent accessible surface loop leads to global changes in repressor function has thus far been difficult to establish.

Our research has focused on identifying the structural and dynamics features at the origin of the long-range, nonlocal perturbations observed in L75F-TrpR, and that may be at the origin of its altered ligand binding functions. We have sought to understand how another mutation (A77V), two residue positions from the L75F mutation in the TrpR sequence and occurring in a similar solvent accessible region of the protein, can yield such a different TrpR variant with significantly distinct L-Trp and DNA ligand binding properties and phenotypes.

Toward these aims, the three-dimensional (3D) solution structure of apo-L75F-TrpR was first determined by NMR [Protein Data Bank (PDB) entry 2XDI] and revealed that the ts apo-L75F-TrpR variant and apo-WT-TrpR are structurally very similar (*34*). Despite very similar overall 3D folds, significant $^{15}N-^1H$ chemical shift differences were observed in two-dimensional (2D) $^1H-^{15}N$ correlation NMR spectra of L75F-TrpR versus WT-TrpR recorded under identical conditions. Such chemical shift changes could not be solely rationalized by near neighbor and ring current effects resulting from the introduction of a phenylalanine side chain at position 75 in L75F-TrpR (*34*). The 3D solution structure of apo-L75F-TrpR thus provided support for the notion that nonlocal long-range effects observed in L75F-TrpR originate from subtle changes in the molecular flexibility of the protein, which we have aimed to characterize in this study using ^{15}N solution NMR relaxation methods.

Heteronuclear NMR is a powerful approach to characterize the internal motions of proteins because ^{15}N, ^{13}C, and $^2H/^1H$ NMR relaxation experiments provide site-specific probes of backbone and side chain atom motions on a wide range of time scales (from picoseconds to milliseconds) (*35*−*39*). Herein, the internal dynamics of N−H amide bond vectors on fast (picosecond to nanosecond) time scales of apo-L75F-TrpR, apo-A77V-TrpR, and apo-WT-TrpR were probed using ^{15}N NMR relaxation experiments (^{15}N-T_1, ^{15}N-T_2, and $^{15}N-\{^1H\}$-nOe) recorded under identical temperature, pH, and buffer conditions.

Comparison of backbone amide dynamics in these three proteins reveals that most of the differences in protein flexibility are observed for backbone amides located in the helix D−turn−helix E DNA-binding domain of the three aporepressors. Analysis of reduced spectral density functions [$J_{eff}(0)$, $J(\omega_N)$, and $J(0.87\omega_H)$] calculated from measured ^{15}N-T_1, ^{15}N-T_2, and

$^{15}N-\{^1H\}$-nOe data for the three apo-TrpR proteins provides evidence that supports the idea that single-amino acid substitutions in the HTH DNA-binding domain of TrpR cause distinct changes in protein dynamics. These findings support the notion that differences in molecular flexibility contribute in part to the altered L-Trp corepressor binding function of L75F-TrpR and A77V-TrpR compared to that of WT-TrpR. Differences in backbone amide dynamics between apo-L75F-TrpR and apo-WT-TrpR are, however, not uniform across the helix D−turn−helix E region. Such observations provide a possible framework for rationalizing why apo-L75F-TrpR has a 10-fold lower L-Trp binding affinity compared to that of apo-WT-TrpR.

Further, we report that the dynamics profiles of backbone amides located in the HTH region of apo-L75F-TrpR differ from those of corresponding amides of apo-A77V-TrpR. Such differences, although subtle, provide a possible explanation for why these two TrpR mutants have such distinct L-Trp corepressor binding properties, even though both variants result from a single conservative amino acid substitution at residue positions very close to each other in the TrpR sequence and both within the solvent accessible HTH DNA-binding domain of TrpR.

MATERIALS AND METHODS

Protein Sample Preparations. ^{15}N NMR relaxation experiments, including measurements of ^{15}N-T_1, ^{15}N-T_2, and $^{15}N-\{^1H\}$-nOes, were conducted on uniformly ^{15}N-labeled samples of apo-L75F-TrpR, apo-A77V-TrpR, and apo-WT-TrpR, prepared according to published protocols (*34*). Briefly, uniformly ^{15}N-labeled L75F-TrpR and WT-TrpR were isolated from *E. coli* strains CY15075 and CY15071 transformed with the overproducing plasmids pJPR2.L75F and pJPR2.WT, respectively. The strains were grown in M9 minimal medium enriched with $[^{15}N]NH_4Cl$ (99% ^{15}N enriched, CIL, Cambridge, MA) as the sole source of nitrogen.

A plasmid encoding the A77V-TrpR mutant, pJPR2.AV77, was engineered using site-directed mutagenesis and pJPR2.WT as a DNA template. Uniformly ^{15}N-enriched or ^{15}N- and ^{13}C-enriched A77V-TrpR was isolated from CY15071 transformed with overproducing plasmid pJPR2.A77 V (*40*). ^{15}N- and ^{13}C-labeled apo-A77V-TrpR was used to record 3D (^1H, ^{15}N, and ^{13}C) NMR experiments to obtain resonance assignments more complete than those available from published work (*29*). ^{15}N- and ^{13}C-labeled apo-WT-TrpR was also expressed in CY15071 cells to obtain a complete list of $^{15}N-^1H$ backbone amide resonance assignments recorded under conditions identical to those used for the structure determination of apo-L75F-TrpR (*34*) and consistent with the buffer conditions used for ^{15}N NMR relaxation studies on all three aporepressors.

The CY15071 *E. coli* cell cultures were supplemented with 20 mL of a 0.2 M unlabeled threonine stock solution per liter to compensate for the fact that this cell strain cannot synthesize threonine de novo. As a result, TrpR samples produced from CY15071 bacterial cells lacked ^{15}N-labeled or ^{15}N- and ^{13}C-labeled threonine (Thr) residues, and signals from these residues could not be observed in ^{15}N-edited or ^{13}C-edited NMR experiments. CY15071 cells transfected with either pJPR2.A77V or pJPR2.WT were grown in M9 minimal medium supplemented with unlabeled Thr, and ^{15}N-labeled ammonium chloride and $^{13}C_6$-labeled glucose as sources of nitrogen and carbon, respectively, to produce uniformly ^{15}N-labeled or ^{15}N- and ^{13}C-labeled A77V-TrpR and WT-TrpR, respectively.

TrpR protein purification was conducted as described by Jin et al. (*30*). For NMR resonance assignment and ^{15}N NMR relaxation experiments, protein samples were prepared in an NMR buffer consisting of 500 mM NaCl, 50 mM sodium phosphate, 1 mM EDTA, 0.01% sodium azide, and a 95% H_2O/5% D_2O mixture (pH 5.7).

NMR Spectroscopy. Sequential ^1H, ^{15}N, and ^{13}C backbone chemical shift assignments of apo-WT-TrpR and apo-A77V-TrpR were performed using uniformly ^{15}N- and ^{13}C-labeled apo-TrpR proteins dissolved in NMR buffer at pH 5.7 to a final protein monomer concentration of ~0.8−1 mM. Triple-resonance (^1H, ^{15}N, and ^{13}C) multidimensional NMR experiments were conducted at 318 K (45 °C) on a Bruker DRX600 spectrometer equipped with a triple-resonance probe and triple-axis pulsed field gradients. Two-dimensional $^1H-^{15}N$ HSQC (*41*) spectra were acquired with spectral widths of 13 ppm in the ^1H (t_2) and 30 ppm in the ^{15}N (t_1) dimensions, with proton and nitrogen carrier frequencies set to 4.6 and 116 ppm, respectively. The 2D NMR spectra were recorded with 1024 and 128 complex points in t_2 and t_1, respectively, using a Waltz-16 (*42*) pulse sequence scheme for ^{15}N decoupling during data acquisition.

Sequential ^1H, ^{15}N, and ^{13}C backbone chemical shift assignments were extracted from a series of heteronuclear (^1H, ^{15}N, and ^{13}C) 3D NMR experiments, including CBCACONH (*43*), HNCA (*44*), and HNCACB (*45*), acquired with spectral widths of 12 ppm (in the ^1H, t_3 dimension), 67 ppm (and 24 ppm for the HNCA experiment) (in the ^{13}C, t_2 dimension), and 30 ppm (in the ^{15}N, t_1 dimension). Data were collected with 512, 128, and 32 complex points in t_3, t_2, and t_1, respectively. ^1H, ^{15}N, and ^{13}C chemical shift dimensions were indirectly referenced to DSS. All NMR spectra were processed using NMRPipe (*46*) and analyzed using SPARKY (*47*). Similar apodization functions were used in all spectral dimensions, using shifted sine bell functions.

Backbone amide ^{15}N NMR relaxation experiments including ^{15}N-T_1, ^{15}N-T_2, and heteronuclear $^{15}N-\{^1H\}$-nOe were conducted at 45 °C in triplicate for all three apo-TrpR proteins using standard NMR pulse sequences (*48*−*50*) at protein concentrations of ~0.8−1 mM. Concentration effects on the ^{15}N NMR relaxation of apo-L75F-TrpR and apo-A77V-TrpR were investigated by recording ^{15}N-T_2 values at lower protein concentrations of 0.6 and 0.4 mM (dimer). The ^{15}N-T_2 relaxation profiles recorded with lower protein concentrations were found to be within experimental error, no different from the ^{15}N-T_2 profiles measured on the ~0.8−1.0 mM protein samples, thus ruling out concentration effects. Previous ^{15}N NMR relaxation studies by Zheng et al. on apo-WT-TrpR were conducted at protein concentrations of 4.6 mM (monomer) (i.e., 2.3 mM dimer), well above the concentration of 1 mM (dimer) used in this work, and did not report any concentration effects (*19*). Moreover, ^{15}N-T_2 values reported for core residues by Zheng et al. are comparable to those measured herein. These experiments demonstrated that the ^{15}N NMR relaxation parameters measured for all three aporepressors are not influenced by the millimolar concentrations used in these studies.

In addition to conducting experiments at 45 °C, we recorded a triplicate series of $^{15}N-\{^1H\}$-nOe measurements for apo-L75F-TrpR at 37 °C, the nonpermissive temperature of the temperature-sensitive (ts) phenotype of the L75F-TrpR variant, to verify that the $^{15}N-\{^1H\}$-nOe profiles observed at 45 °C (a temperature slightly above the permissive temperature, 42 °C, of the ts phenotype of L75F-TrpR) are comparable to those recorded at the nonpermissive temperature of 37 °C.

^{15}N-T_1 relaxation profiles were sampled at seven different relaxation delay time points of 40, 96, 200, 400, 600, 1000, and 1200 ms. ^{15}N-T_2 relaxation profiles were sampled at eight different relaxation delay periods of 8, 16, 32, 40, 64, 80, 104, and 152 ms, with the delay between the series of ^{15}N 180° pulses applied in the CPMG sequence set to 0.5 ms (*51*, *52*). For both ^{15}N-T_1 and ^{15}N-T_2 measurements, the data were collected using 512 complex points in the ^{1}H acquisition time dimension (t_2) and 256 complex data points in the ^{15}N t_1 indirect time evolution dimension, using a WALTZ-16 ^{15}N decoupling scheme during data acquisition. ^{15}N-T_1 and ^{15}N-T_2 values were calculated from the series of NMR spectra by nonlinear regression analysis of single-exponential decays of resonance intensities. Errors in ^{15}N-T_1 and ^{15}N-T_2 were estimated by Monte Carlo calculation (*53*).

^{15}N−{^{1}H}-nOes were measured using a water-flip-back 2D heteronuclear NOE pulse sequence and the results corrected for the finite repetition delay according to the method of Grzesiek and Bax (*50*). Heteronuclear ^{15}N−{^{1}H}-nOes were established as the ratio of peak intensities (I/I_o) from NMR data sets acquired with (I) or without (I_o) solvent presaturation (*50*). ^{15}N−{^{1}H}-nOe spectra were recorded using 1024 and 256 complex data points in t_2 and t_1, respectively, using 48 scans per t_1 increment. The ^{15}N−{^{1}H}-nOe experiments were recorded using a delay of 4.5 s between scans to minimize the introduction of systematic errors in measured ^{15}N−{^{1}H}-nOes that could be produced by incomplete signal recovery and solvent saturation (*50*). To minimize the impact of magnetic field drift, ^{15}N-T_2 and ^{15}N−{^{1}H}-nOe data were collected in an interleaved manner, while 2D ^{15}N-T_1 data sets were acquired consecutively using a list of shuffled relaxation delay time points.

Processing of NMR Spectra. All NMR spectra were processed using NMRPipe/NMRDraw and SPARKY (*46*, *47*). Apodization was performed in both dimensions using a Lorentz-to-Gauss window function, consisting of a combination of an inverse exponential and a Gaussian line broadening function. The purpose of applying a Lorentz-to-Gauss line shape function (rather than sine bell functions) is to replace the exponential decay of the original data with a Gaussian decay so that following Fourier transformation (FT), the NMR signals adopt Gaussian-like line shapes rather than Lorentzian line shapes. Application of this particular line broadening function (specified by the GM command in NMRPipe and g_1 and g_2 input parameters) was necessary for accurate fitting of NMR signal intensities using the nonlinear least-squares nlinLS function of NMRPipe (*46*). Typical values of g_1 (exponential term) and g_2 (Gaussian line broadening term) used for processing of the NMR relaxation data for TrpR were 10 and 15 Hz, respectively, for processing of the t_2 (acquisition) dimension and 6 and 12 Hz, respectively, for processing of the t_1 (indirect) dimension of the 2D ^{1}H−^{15}N NMR relaxation and ^{15}N−{^{1}H}-nOe experiments.

Data processing using NMR peak heights instead of peak volumes yielded comparable relaxation analysis and ^{15}N-T_1 and ^{15}N-T_2 profiles. The two spectral analysis approaches were used to establish that the final results (i.e., ^{15}N-T_1, ^{15}N-T_2, and ^{15}N−{^{1}H}-nOes) were insensitive to whether the "raw data" consisted of integrated intensities or peak heights.

Errors associated with determination of ^{15}N-T_1, ^{15}N-T_2, and ^{15}N−{^{1}H}-nOe values represented one standard deviation among triplicate sets of measurements. These errors were consistent with those calculated by Monte Carlo simulations or spectral noise estimates (in the case of ^{15}N−{^{1}H}-nOe measurements) (*54*).

Reduced Spectral Density Mapping and Model-Free Analysis. Reduced spectral density analysis was performed using the following relationships as described by Bracken et al. (*55*):

$$\sigma_{NH} = R_1(\mathrm{NOE}-1)\gamma_N/\gamma_H$$

$$J(0.87\omega_H) = 4\sigma_{NH}/(5d^2)$$

$$J(\omega_N) = (4R_1 - 5\sigma_{NH})/(3d^2 + 4c^2)$$

$$J_{eff}(0) = (6R_2 - 3R_1 - 2.72\sigma_{NH})/(3d^2 + 4c^2)$$

where $d = (\mu_o h\gamma_N\gamma_H/8\pi^2)(r^{-3})$ and $c = \omega_N\Delta\sigma/\sqrt{3}$. γ_N and γ_H are the gyromagnetic ratios of the ^{1}H and ^{15}N nuclei, respectively. ω_N and ω_H are the Larmor frequencies. r is the internuclear ^{1}H−^{15}N distance (1.02 Å), and $\Delta\sigma$ is the ^{15}N CSA (−160 ppm). The subscript in $J_{eff}(0)$ refers to an "effective" $J(0)$, which is uncorrected for chemical exchange effects (*55*, *56*). Reported error bars were calculated from propagation of experimental errors determined for the measured ^{15}N-T_1, ^{15}N-T_2, and ^{15}N−{^{1}H}-nOe series.

Analysis of ^{15}N-T_1, ^{15}N-T_2, and ^{15}N−{^{1}H}-nOe values in terms of reduced spectral density functions [$J_{eff}(0)$, $J(\omega_N)$, and $J(0.87\omega_H)$] has the advantage that these functions are sensitive to frequencies of motions (*57*) rather than amplitudes of motions. As mentioned, $J(0)$ contains a contribution from chemical exchange (R_{exch}) which, when present, affects ^{15}N-T_2 parameters. Our ^{15}N NMR relaxation data, recorded at a single magnetic field strength of 14.1 T, precluded explicit calculations of R_{exch}, thus leading us to report $J_{eff}(0)$ [corresponding to $J(0)$ uncorrected for R_{exch}]. High $J_{eff}(0)$ values indicated the presence slow (microseconds to milliseconds) motions, whereas $J(0.87\omega_H)$ values were sensitive only to fast picosecond to nanosecond internal motions (*58*).

Using reduced spectral density functions obtained for backbone amides of the core helices of the aporepressors, an apparent correlation time (τ_m) for overall reorientation of the molecules was calculated as follows (*55*):

$$\tau_m = \omega_N{}^{-1}\{[J_{eff}(0) - J(\omega_N)]/J(\omega_N)\}^{1/2}$$

and yielded τ_m values of 10.53, 10.42, and 10.43 ns for apo-L75F-TrpR, apo-WT-TrpR, and apo-A77V-TrpR, respectively. These values are in good agreement with those calculated using FastModelFree analysis described below.

The ^{15}N NMR relaxation data were also analyzed using FastModelFree (*59*), an interface to ModelFree (*60*), which is based on the model-free approach of Lipari and Szabo (*61*, *62*) and analyzes ^{15}N NMR relaxation parameters in terms of internal motions of amide N−H bond vectors in the presence of anisotropic overall diffusion of the proteins. The analysis consisted of first estimating the correlation time for overall molecular reorientation from the mean of 10% trimmed ^{15}N-T_1/^{15}N-T_2 ratios [prescreened using the method of Nicholson et al. (*54*) and Pawley et al. (*63*)] and determining the global tumbling parameters for the proteins from a best fit of these filtered ^{15}N-T_1/^{15}N-T_2 relaxation ratios (*64*). All three TrpR aporepressors yielded ^{15}N-T_1/^{15}N-T_2 relaxation patterns consistent with an axially symmetric prolate model of diffusion, in agreement with previously reported values for WT-TrpR (*19*).

Using ^{15}N-T_1/^{15}N-T_2 ratios and the screening criteria (described in the Supporting Information), initial estimates of $D_{\parallel}/D_{\perp}$ (1.12) and τ_m (10.0 ns) for apo-L75F-TrpR, apo-A77V-TrpR, and apo-WT-TrpR protein molecules were used as input in the FastModelFree calculations. Following FastModelFree optimization of global diffusion parameters, the calculations yielded τ_m values of 10.45 ± 0.05 ns for apo-L75F-TrpR, 10.12 ± 0.10 ns for apo-WT-TrpR, and 10.15 ± 0.04 ns for apo-A77V-TrpR and ratios of parallel to perpendicular principal components of the diffusion tensor ($D_{\parallel}/D_{\perp}$) for anisotropic diffusion of 1.21 ± 0.03 for apo-L75F-TrpR, 1.28 ± 0.08 for apo-WT-TrpR, and 1.19 ± 0.03 for apo-A77V-TrpR. Following determination of the global diffusion parameters, FastModelFree calculations were performed according to the method of Mandel et al. (*61*, *62*, *64*) to yield internal motional parameters, including S^2 generalized order parameters, the internal correlation time for N−H bond vector motion, τ_e, and the chemical exchange contribution to relaxation, R_{exch}.

^{15}N NMR relaxation parameters, reduced spectral density functions, FastModelFree-derived motional parameters, and chemical shift data have been deposited in the BioMagResBank as entries 17010 for apo-WT-TrpR, 17012 for apo-L75F-TrpR, and 17013 for apo-A77V-TrpR.

RESULTS

Resonance Assignments of Backbone Amides of Apo-WT-TrpR and Apo-A77V-TrpR. Multidimensional (2D and 3D) heteronuclear (^{1}H, ^{15}N, and ^{13}C) NMR experiments were employed to assign NMR resonances originating from the ^{1}H, ^{15}N, and ^{13}Cα/β backbone atoms of apo-WT-TrpR and apo-A77V-TrpR. Analysis of 3D HNCACB, CBCACONH, and HNCA data sets permitted the assignment of 85 and 88 backbone amides of a total of 104 non-proline backbone residues in apo-WT-TrpR and apo-A77V-TrpR, respectively. Other observed signals were not assigned because of extensive resonance overlaps of these amides. Resonance assignments of backbone atoms (^{1}H, ^{15}N, and ^{13}Cα/β) obtained for apo-WT-TrpR and apo-A77V-TrpR have been deposited as BioMagResBank entries 17010 and 17013, respectively. Resonance assignments for apo-L75F-TrpR were obtained from published work (*34*). In this case, 101 of 104 non-proline residues had been assigned (*34*).

^{15}N NMR Relaxation, ^{15}N-T_1, ^{15}N-T_2, and ^{15}N−{^{1}H}-nOe Measurements. ^{15}N/^{1}H backbone amide dynamics studies were performed on uniformly ^{15}N-labeled samples of apo-L75F-TrpR, apo-WT-TrpR, and apo-A77V-TrpR using 2D ^{1}H−^{15}N NMR relaxation experiments as described above. Series of ^{15}N-T_1, ^{15}N-T_2, and ^{15}N−{^{1}H}-nOe parameters were measured in triplicate on each TrpR aporepressor to assess the reproducibility of the data and to estimate the precision of the measurements. ^{15}N-T_1, ^{15}N-T_2, and ^{15}N−{^{1}H}-nOe parameters were measured for 93 backbone amides of apo-L75F-TrpR, 72 of apo-WT-TrpR, and 80 of apo-A77V-TrpR. NMR resonances originating from NH groups located within the helix D−turn−helix E DNA-binding domains of all three aporepressors were more difficult to characterize as many displayed NMR signals that overlapped significantly, precluding accurate determination of integrated peak intensities or peak volumes. Of 23 backbone amides located within the stretch of residues 68−90 (i.e., the helix D−turn−helix E region of the repressors), reliable ^{15}N NMR relaxation parameters could be established for 19, 11, and 13 NH backbone amides located within this region of apo-L75F-TrpR, apo-WT-TrpR, and apo-A77V-TrpR, respectively. The number of ^{15}N−{^{1}H}-nOes measured for helix E amides of apo-A77V-TrpR was particularly sparse because of substantial NMR resonance overlaps precluding accurate measurements of resonance intensities.

^{15}N NMR Relaxation Profiles for Backbone Amides of the Two Apo-TrpR Variants Compared to Those of Apo-WT-TrpR. Measured backbone amide ^{15}N-T_1, ^{15}N-T_2, and ^{15}N−{^{1}H}-nOe parameters for apo-L75F-TrpR and apo-A77V-TrpR are shown in comparison with those of apo-WT-TrpR in Figures 1 and 2, respectively. These figures depict the average ^{15}N-T_1, ^{15}N-T_2, and ^{15}N−{^{1}H}-nOe parameters for all measurable amide residues. Complete lists of all relaxation parameters measured for apo-L75F-TrpR, apo-WT-TrpR, and apo-A77V-TrpR are given in Tables S2−S4, respectively, of the Supporting Information. In general, measured ^{15}N-T_1 and ^{15}N-T_2 values observed for all three aporepressors are within the theoretically expected range for the 25 kDa size of TrpR.

The ^{15}N-T_1 and ^{15}N-T_2 NMR relaxation time constants of NH residues located in the core helices (helix A, residues 16−32; helix B, residues 35−42; helix C, residues 45−63; and helix F, residues 93−103) of the proteins were found to be quite uniform for all three aporepressors. Via comparison of the ^{15}N-T_1 and ^{15}N-T_2 data for apo-L75F-TrpR and apo-WT-TrpR, ^{15}N-T_1 yielded an average of 837 ± 37 ms while ^{15}N-T_2 yielded an average of 73 ± 4 ms (Figure 1A,B). Similar uniform ^{15}N-T_1 and ^{15}N-T_2 trends were observed for backbone amides in core helices of apo-A77V-TrpR and apo-WT-TrpR (Figure 2A,B), yielding average values for ^{15}N-T_1 and ^{15}N-T_2 of 840 ± 40 and 75 ± 5 ms, respectively (see Tables S3 and S4 of the Supporting Information for residue-specific ^{15}N NMR relaxation values).

Measured ^{15}N-T_1 values were also quite uniform for backbone amides residing in the helix D−turn−helix E DNA-binding domain of all three proteins, and not significantly distinct from ^{15}N-T_1 values measured for backbone amides of core helices (mean ^{15}N-T_1 of 790 ± 50 ms). A greater distribution of ^{15}N-T_2 values was, however, observed for residues in this same region (residues 68−90) of the three aporepressors (see Table 1 and Tables S2−S4 of the Supporting Information). ^{15}N-T_2 values were slightly elevated (mean ^{15}N-T_2 of 85 ± 5 ms) for backbone amides within the HTH domain of all three apo-TrpR proteins. A greater scatter in ^{15}N-T_2 data was observed for helix E amides of apo-L75F-TrpR compared to those of the other two aporepressors (Figures 1B and 2B). The break in the uniformity of ^{15}N-T_2 trends was also slightly different for the three proteins, starting approximately at residue L62 and ending approximately at residue L89 for apo-L75F-TrpR versus starting at residues G52 and G64 and ending at residues N87 and S86 for apo-WT-TrpR and apo-A77V-TrpR, respectively (Figures 1B and 2B). The potential significance of such deviations in ^{15}N-T_2 trends for backbone amides of the HTH region of the three proteins is unclear. An interesting possibility is that some residues of the HTH domain may be undergoing chemical exchange and experiencing slower microsecond to millisecond time scale motions in addition to the fast picosecond to nanosecond motions probed by measurement of ^{15}N-T_1. Complex motions in the HTH domains could lead to greater spread in ^{15}N-T_2 relaxation time constants. More rigorous analysis of the three proteins using ^{15}N-T_1/T_2 ratios identified two residues (I82 and L89) in apo-L75F-TrpR and two residues (E60 and G64) in apo-WT-TrpR undergoing chemical exchange. These results were confirmed with additional ^{15}N-$T_{1\rho}$ experiments that yielded high ^{15}N-$T_{1\rho}/T_2$ ratios for these

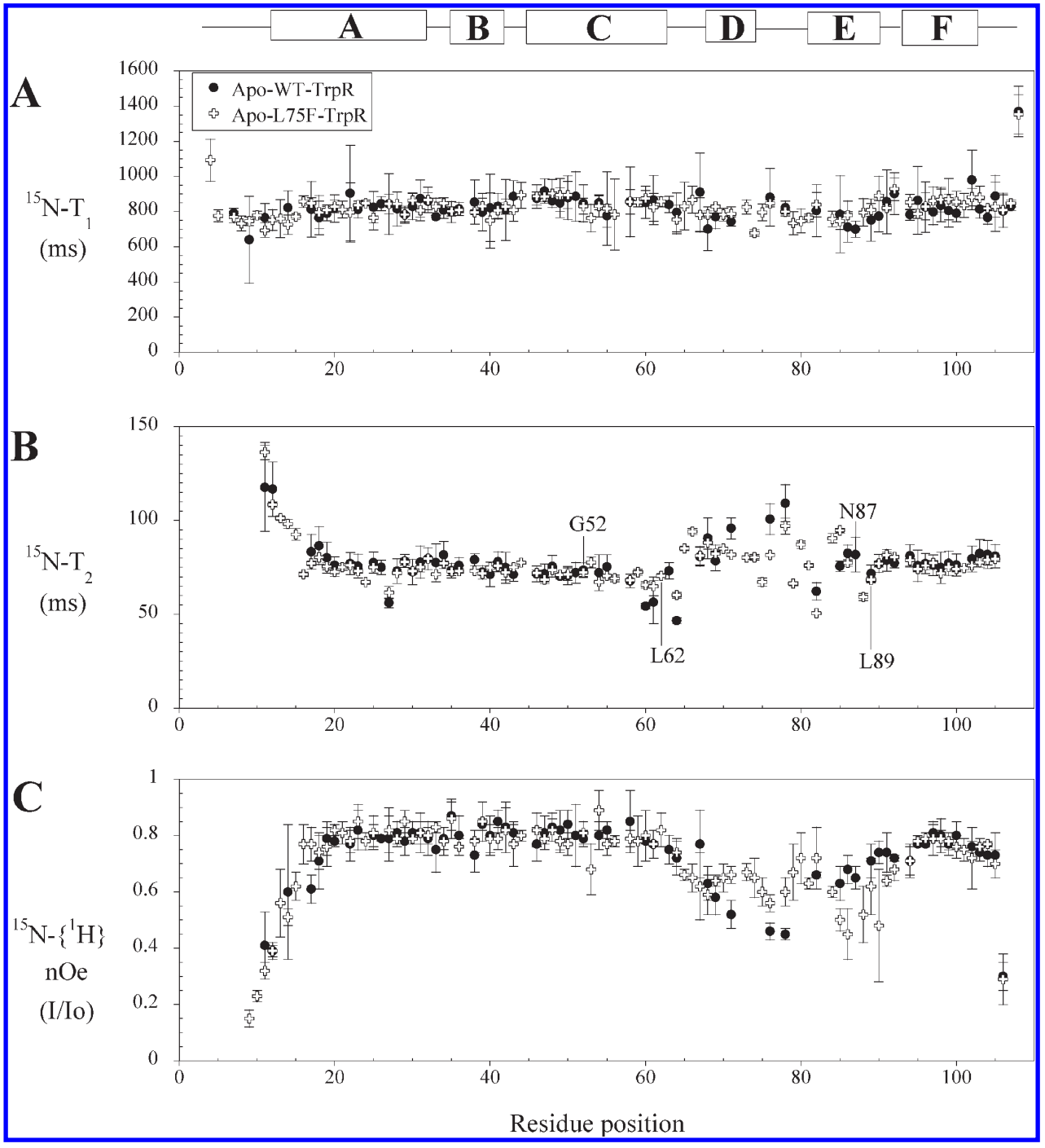

FIGURE 1: Comparison plots of ^{15}N relaxation parameters as a function of residue number between apo-L75F-TrpR and apo-WT-TrpR: (A) ^{15}N-T_1, (B) ^{15}N-T_2, and (C) ^{15}N−{^{1}H}-nOe measured for apo-WT-TrpR (filled circles) and apo-L75F-TrpR (open crosses) recorded at a magnetic field strength of 14.1 T. Plotted error bars correspond to errors reported in Tables S2 and S3 of the Supporting Information and calculated as described in the text. Secondary structure elements of the two aporepressors are depicted above the plots. ^{15}N NMR relaxation profiles are quite uniform for backbone amides located in the core A−C and F α-helices. ^{15}N-T_1 trends for apo-L75F-TrpR are very similar to those of apo-WT-TrpR. Significant differences are observed in the ^{15}N-T_2 and ^{15}N−{^{1}H}-nOe trends for amides located within the helix D−turn−helix E DNA-binding domain of the two aporepressors.

residues of apo-L75F-TrpR and apo-WT-TrpR, respectively (data not shown). In addition, the ^{15}N-$T_{1\rho}/T_2$ ratios also identified G85 in apo-WT-TrpR as a residue undergoing chemical exchange. In fact, the most interesting inference of these experiments is that chemical exchange can be traced to two different locations in apo-WT-TrpR, suggesting that the wild-type protein has two "pivot points", one at the C-terminus of helix C (residues E60 and G64) and the second in the middle of helix E (G85), whereas the Leu to Phe mutation in apo-TrpR at position 75 manifests itself in reduced slow time scale exchange motions on helix C as noticed from the high ^{15}N-$T_{1\rho}/T_2$ ratio observed for only I82 located on the N-terminus of helix E for apo-L75F-TrpR.

Significantly larger ^{15}N-T_1 and ^{15}N-T_2 values were measured for backbone amides located in the N- and C-termini of all three aporepressors. This is consistent with structural data indicating that these segments of the proteins are disordered and in all likelihood highly flexible (*16*, *34*).

Similarly, measured heteronuclear ^{15}N−{^{1}H}-nOes were quite uniform for backbone amides located in the core A−C and F α-helices of apo-L75F-TrpR, apo-WT-TrpR, and apo-A77V-TrpR,

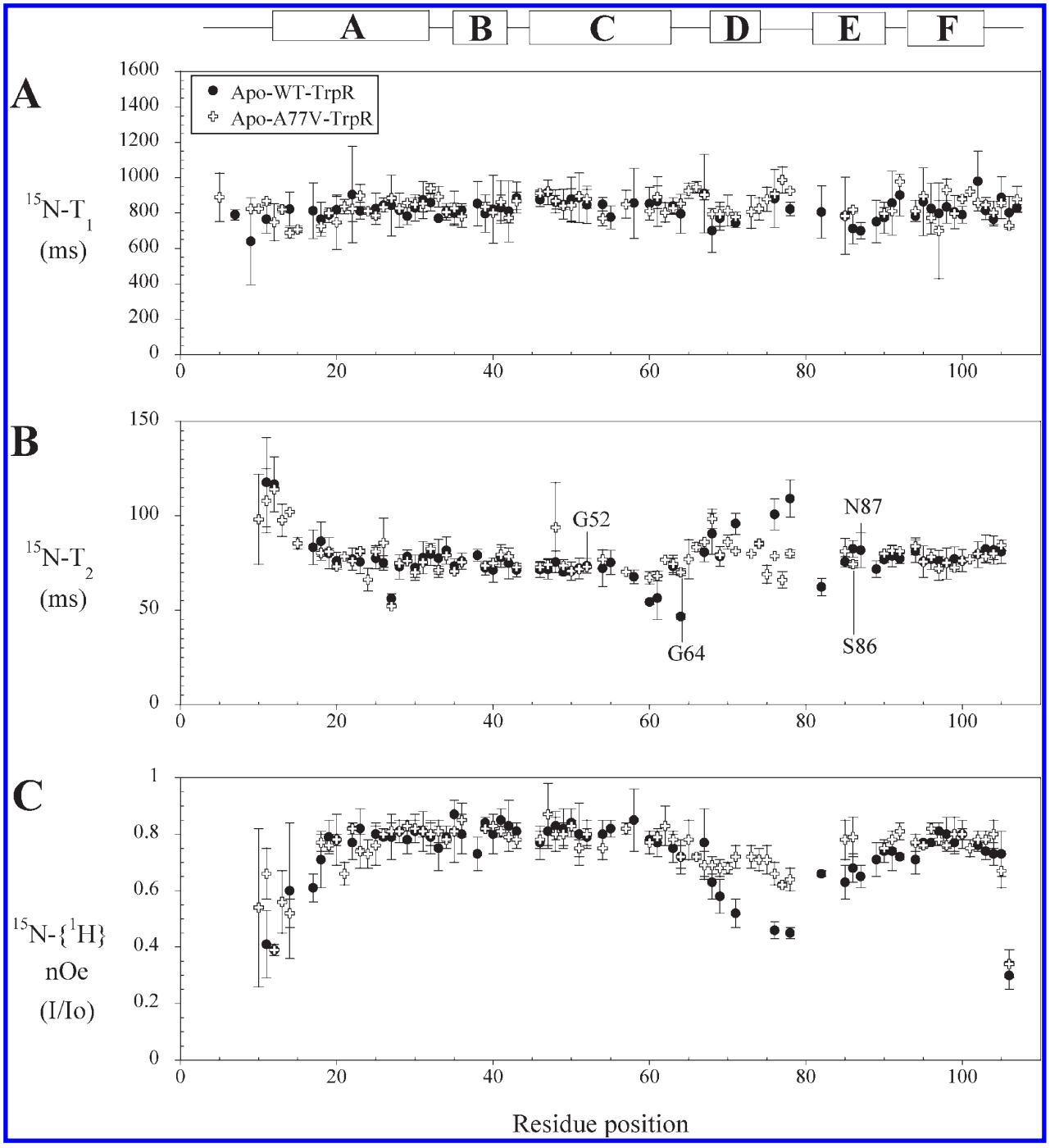

FIGURE 2: Comparison plots of ^{15}N relaxation parameters as a function of residue number between apo-A77V-TrpR and apo-WT-TrpR: (A) ^{15}N-T_1, (B) ^{15}N-T_2, and (C) ^{15}N−{^{1}H}-nOe measured for apo-WT-TrpR (filled circles) and apo-A77V-TrpR (open crosses) recorded at a magnetic field strength of 14.1 T. Plotted error bars correspond to errors reported in Tables S3 and S4 of the Supporting Information and calculated as described in the text. The proteins' secondary structure is represented above the plots. Less scatter is observed in the relaxation profiles of apo-A77V-TrpR. ^{15}N-T_1 trends for the super-repressor are very similar to those of apo-WT-TrpR. However, major differences are observed in the ^{15}N-T_2 and ^{15}N−{^{1}H}-nOe trends of backbone amides residing within the helix D−turn−helix E region of the two aporepressors. Most prominent are differences seen for amides of the helix D−turn segment of the HTH DNA-binding domain.

with little spread from mean I/I_o values of ~0.80 ± 0.04 (Figures 1C and 2C and Tables S2−S4 of the Supporting Information). More significant ^{15}N−{^{1}H}-nOe differences among the three aporepressors were observed for backbone amides located in their helix D−turn−helix E DNA-binding domains. Measured ^{15}N−{^{1}H}-nOes were significantly lower (by ~0.20 or more) than those measured for backbone amides in core helices. The lower ^{15}N−{^{1}H}-nOe patterns differ for the three aporepressors and were not uniform across helices D and E (see Figures 1C and 2C and Table 1). ^{15}N−{^{1}H}-nOes for helix D amides of apo-L75F-TrpR clustered around a mean value of ~0.60, while helix E amides exhibited lower ^{15}N−{^{1}H}-nOes of ~0.50 (Table 1). In contrast, ^{15}N−{^{1}H}-nOes for helix D amides and the turn region of apo-WT-TrpR (~0.45) were lower than those of apo-L75F-TrpR (~0.60) (Figure 1C), suggesting that helix D of apo-WT-TrpR is more flexible on a picosecond to nanosecond time scale than that of apo-L75F-TrpR (Table 1). The flexibility pattern seemed to be reversed for helix E amides, where ^{15}N−{^{1}H}-nOes were higher for helix E amides of apo-WT-TrpR (~0.70) than for apo-L75F-TrpR (~0.55). The overall lower ^{15}N−{^{1}H}-nOe trends clearly indicated

Table 1: Spectral Density Parameters[a] Obtained for Amides E65−W99 That Comprise Residues within the Helix D−Turn−Helix E DNA-Binding Domain (Q68−K90) of the Trp Aporepressors and Display the Largest Variations

	apo-L75F-TrpR				apo-WT-TrpR				apo-A77V-TrpR		
residue	$J_{eff}(0)$ (ns/rad)	$J(\omega_N)$ (ns/rad)	$J(0.87\omega_H)$ (ps/rad)	residue	$J_{eff}(0)$ (ns/rad)	$J(\omega_N)$ (ns/rad)	$J(0.87\omega_H)$ (ps/rad)	residue	$J_{eff}(0)$ (ns/rad)	$J(\omega_N)$ (ns/rad)	$J(0.87\omega_H)$ (ps/rad)
E65	4.24 ± 0.07	0.30 ± 0.04	6.47 ± 0.94	E65	−	−	−	E65	4.78 ± 0.66	0.27 ± 0.01	3.71 ± 1.24
M66	3.83 ± 0.07	0.28 ± 0.02	6.33 ± 0.98	M66	−	−	−	M66	4.36 ± 0.13	0.26 ± 0.01	4.63 ± 0.23
S67	4.45 ± 0.28	0.32 ± 0.05	7.71 ± 2.50	S67	−	−	−	S67	4.21 ± 0.05	0.27 ± 0.01	5.37 ± 0.86
Q68	4.07 ± 0.17	0.31 ± 0.01	7.79 ± 1.71	Q68	−	−	−	Q68	3.64 ± 0.20	0.31 ± 0.01	6.09 ± 0.62
R69	4.4 ± 0.25	0.29 ± 0.01	6.42 ± 0.20	R69	4.62 ± 0.34	0.31 ± 0.03	8.52 ± 1.34	R69	4.56 ± 0.06	0.31 ± 0.03	6.34 ± 0.84
E70	4.23 ± 0.03	0.31 ± 0.01	7.39 ± 0.86	E70	−	−	−	E70	4.19 ± 0.20	0.30 ± 0.03	6.19 ± 0.80
L71	4.42 ± 0.04	0.31 ± 0.01	7.13 ± 0.69	L71	3.72 ± 0.23	0.32 ± 0.01	10.00 ± 1.11	L71	4.44 ± 0.02	0.31 ± 0.01	5.59 ± 0.81
K72	−	−	−	K72	−	−	−	K72	-	-	-
N73	4.52 ± 0.02	0.29 ± 0.01	6.79 ± 0.68	N73	−	−	−	N73	4.53 ± 0.03	0.31 ± 0.04	5.46 ± 1.02
E74	4.45 ± 0.09	0.36 ± 0.01	8.03 ± 2.72	E74	−	−	−	E74	4.24 ± 0.07	0.30 ± 0.02	5.52 ± 0.90
F75	5.43 ± 0.19	0.30 ± 0.02	8.45 ± 0.66	L75	−	−	−	L75	5.31 ± 0.37	0.28 ± 0.02	5.16 ± 0.98
G76	4.44 ± 0.04	0.28 ± 0.01	8.10 ± 0.95	G76	3.57 ± 0.31	0.28 ± 0.06	9.85 ± 2.10	G76	4.62 ± 0.01	0.27 ± 0.01	5.83 ± 0.68
A77	−	−	−	A77	−	−	−	V77	5.58 ± 0.41	0.24 ± 0.02	5.99 ± 0.53
G78	3.69 ± 0.18	0.30 ± 0.01	7.99 ± 1.57	G78	3.27 ± 0.30	0.29 ± 0.01	10.50 ± 0.67	G78	4.56 ± 0.12	0.26 ± 0.01	6.06 ± 0.67
I79	5.48 ± 0.09	0.33 ± 0.03	7.05 ± 3.56	I79	−	−	−	I79	−	−	−
A80	4.11 ± 0.10	0.33 ± 0.03	6.32 ± 1.64	A80	−	−	−	A80	−	−	−
T81	4.77 ± 0.07	0.32 ± 0.01	7.15 ± 0.31	T81	−	−	−	T81	−	−	−
I82	7.31 ± 0.06	0.30 ± 0.02	4.87 ± 1.39	I82	5.88 ± 0.36	0.31 ± 0.05	6.74 ± 1.11	I82	−	−	−
T83	−	−	−	T83	−	−	−	T83	−	−	−
R84	3.95 ± 0.12	0.32 ± 0.02	8.24 ± 0.79	R84	−	−	−	R84	−	−	−
G85	3.76 ± 0.06	0.32 ± 0.02	10.70 ± 0.75	G85	4.17 ± 1.39	0.33 ± 0.10	7.79 ± 2.67	G85	4.46 ± 0.39	0.31 ± 0.01	4.36 ± 1.39
S86	4.67 ± 0.11	0.30 ± 0.03	12.30 ± 1.83	S86	4.36 ± 0.25	0.35 ± 0.04	7.09 ± 1.40	S86	4.89 ± 0.13	0.30 ± 0.01	4.00 ± 1.31
N87	−	−	−	N87	4.43 ± 0.53	0.35 ± 0.02	7.81 ± 1.04	N87	−	−	−
S88	6.18 ± 0.20	0.30 ± 0.03	11.10 ± 1.27	S88	−	−	−	S88	−	−	−
L89	5.32 ± 0.12	0.30 ± 0.01	8.70 ± 1.76	L89	5.06 ± 0.31	0.33 ± 0.05	6.11 ± 1.69	L89	−	−	−
K90	4.73 ± 0.33	0.28 ± 0.03	6.40 ± 1.58	K90	4.72 ± 0.10	0.32 ± 0.03	5.27 ± 0.99	K90	4.52 ± 0.06	0.31 ± 0.01	4.87 ± 0.43
A91	4.43 ± 0.09	0.30 ± 0.01	7.04 ± 0.41	A91	4.62 ± 0.34	0.30 ± 0.06	4.91 ± 1.69	A91	4.43 ± 0.15	0.30 ± 0.01	4.22 ± 0.55
A92	4.52 ± 0.03	0.26 ± 0.02	5.39 ± 1.08	A92	4.72 ± 0.16	0.28 ± 0.03	4.89 ± 0.59	A92	4.49 ± 0.10	0.25 ± 0.01	3.02 ± 0.47
P93	−	−	−	P93	−	−	−	P93	−	−	−
V94	4.61 ± 0.18	0.29 ± 0.02	5.47 ± 1.67	V94	4.46 ± 0.34	0.31 ± 0.01	5.79 ± 1.05	V94	4.32 ± 0.25	0.30 ± 0.02	4.41 ± 0.69
E95	4.9 ± 0.09	0.31 ± 0.01	4.16 ± 0.24	E95	4.85 ± 0.53	0.29 ± 0.05	4.27 ± 0.81	E95	4.83 ± 0.02	0.27 ± 0.01	4.16 ± 0.17
L96	4.79 ± 0.14	0.30 ± 0.03	3.96 ± 0.68	L96	4.73 ± 0.36	0.30 ± 0.05	4.41 ± 0.68	L96	4.62 ± 0.05	0.32 ± 0.01	3.65 ± 0.43
R97	4.71 ± 0.09	0.29 ± 0.03	2.92 ± 0.61	R97	4.78 ± 0.36	0.31 ± 0.03	3.73 ± 0.67	R97	−	−	−
Q98	5.08 ± 0.04	0.29 ± 0.02	3.98 ± 0.47	Q98	4.91 ± 0.57	0.30 ± 0.03	3.77 ± 1.22	Q98	4.87 ± 0.09	0.27 ± 0.02	4.04 ± 0.33
W99	4.84 ± 0.08	0.29 ± 0.04	3.80 ± 0.74	W99	4.72 ± 0.42	0.31 ± 0.04	4.48 ± 0.95	W99	5.01 ± 0.13	0.31 ± 0.01	3.9 ± 1.19

[a] Spectral density parameters calculated at 14.1 T. See Materials and Methods for equations used to derive them.

that backbone amides in the HTH DNA-binding domains of the aporepressors undergo a greater degree of picosecond to nanosecond internal fluctuations and are therefore more flexible than core amides of both apo-L75F-TrpR and apo-WT-TrpR.

Interestingly, measured $^{15}N-\{^1H\}$-nOes for backbone amides in helices D and E of apo-A77V-TrpR were slightly lower than those measured for core residues (~0.70), but not as low as those measured for corresponding amides of apo-L75F-TrpR and apo-WT-TrpR (Figure 2C and Table 1). This suggests that the helix D−helix E region of apo-A77V-TrpR is not as flexible on a picosecond to nanosecond time scale as that of apo-WT-TrpR or apo-L75F-TrpR. The slightly higher $^{15}N-\{^1H\}$-nOes (relative to those of apo-WT-TrpR and apo-L75F-TrpR) agree with the earlier study by Jardetzky and co-workers (*29*) that indicated that the Ala to Val amino acid substitution at residue 77 stabilizes the HTH domain of A77V-TrpR (*29*).

Analysis of ^{15}N NMR Relaxation Parameters in Terms of Reduced Spectral Density. The ^{15}N NMR relaxation data obtained for apo-WT-TrpR, apo-L75F-TrpR, and apo-A77V-TrpR were analyzed using reduced spectral density mapping (*57*, *65*−*67*) as well as the ModelFree approach (*59*, *60*, *64*). Both types of analysis were undertaken because of the fact that most of the interesting differences in ^{15}N NMR relaxation parameters were found for amides residing in the HTH DNA-binding domain of the three proteins. This region is also the most challenging to probe by NMR because of either the absence of ^{15}N signals as a result of unlabeled threonines added to the CY15071 sample preparations or amide resonance overlap. For all other amides for which reliable ^{15}N-T_1, ^{15}N-T_2, and $^{15}N-\{^1H\}$-nOe data could be obtained, spectral density functions [$J_{eff}(0)$, $J(\omega_N)$, and $J(0.87\omega_H)$] were calculated for each residue of the aporepressors at a single magnetic field strength of 14.1 T. The results are presented in Figures 3 and 4, and a complete collection of reduced spectral density functions is available in Tables S5−S7 of the Supporting Information. As foreshadowed by the trends in ^{15}N-T_1, ^{15}N-T_2, and $^{15}N-\{^1H\}$-nOe values, the reduced spectral density functions $J_{eff}(0)$, $J(\omega_N)$, and $J(0.87\omega_H)$ for N−H bond vectors of the core α-helices of all three aporepressors were found to be fairly uniform, indicating that core amides have very similar motional properties. The $J(\omega_N)$ functions were very similar throughout the sequence of all three proteins (Figures 3B and 4B). These uniform $J(\omega_N)$ patterns are consistent with the uniform trends observed in the ^{15}N-T_1 data and reflect the same insensitivity to residue position. The fact that

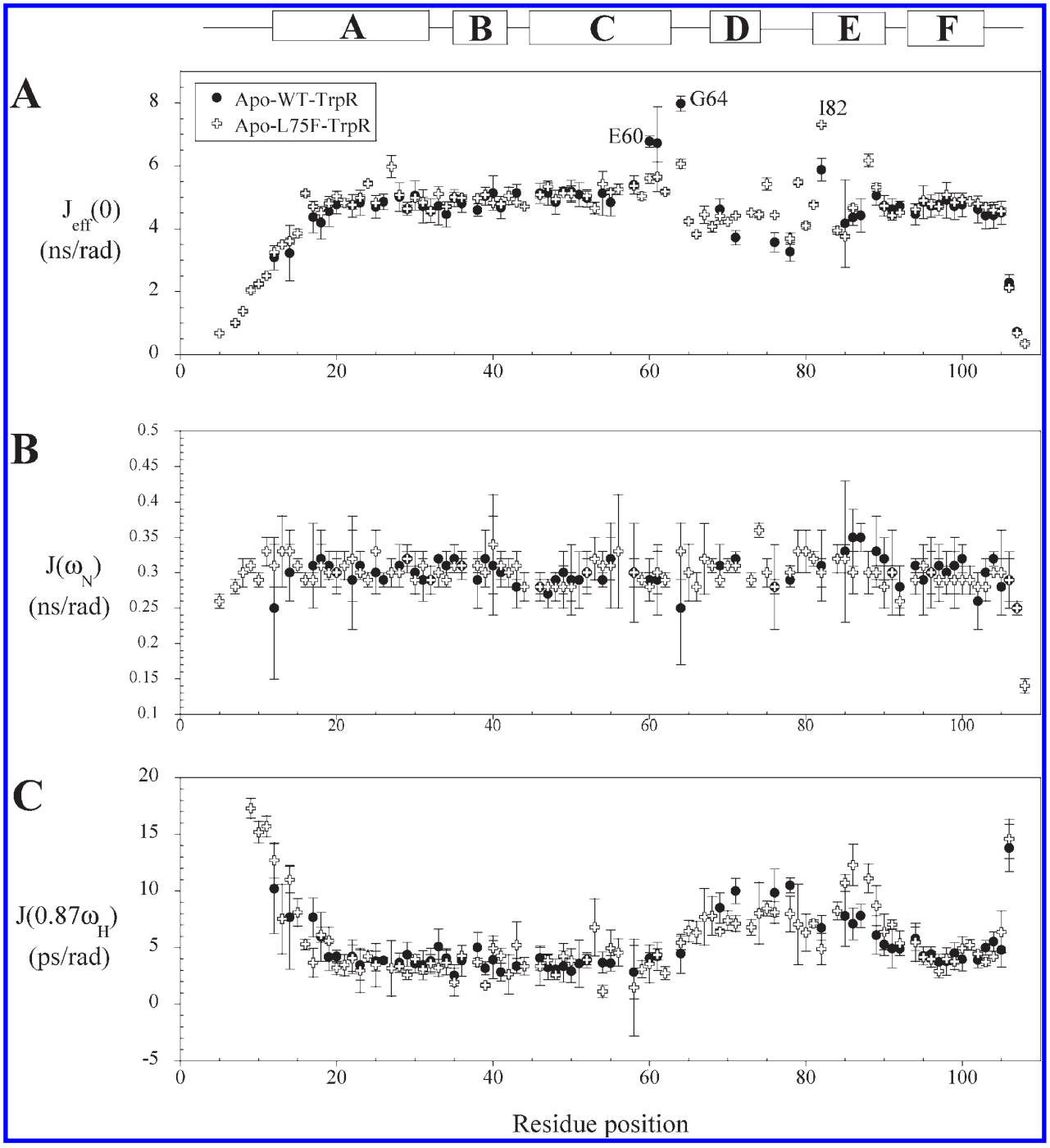

FIGURE 3: Comparison plots of reduced spectral density functions calculated for apo-WT-TrpR (filled circles) and apo-L75F-TrpR (open crosses): (A) $J_{eff}(0)$, (B) $J(\omega_N)$, and (C) $J(0.87\omega_H)$, with secondary structural elements depicted above the plots. Plotted error bars correspond to errors reported in Tables S5 and S6 of the Supporting Information. Residues with high $J_{eff}(0)$ values (suspected to include R_{exch}) from both proteins are labeled in panel A. Significant differences in $J(0.87\omega_H)$ are observed between the two aporepressors for backbone amides of the helix D−turn−helix E motif (C). Slightly elevated $J(0.87\omega_H)$ values for helix D amides of apo-WT-TrpR compared to their counterparts in apo-L75F-TrpR support the notion that helix D of the wild-type aporepressor is more flexible (in terms of picosecond to nanosecond internal motions) than helix D of the ts apo-TrpR mutant. The $J(0.87\omega_H)$ pattern is reversed for helix E, indicating increased flexibility of this region in apo-L75F-TrpR compared to apo-WT-TrpR.

^{15}N-T_1 trends are consistent with $J(\omega_N)$ profiles is not too surprising considering that $J(\omega_N)$ is a measure of the spectral power of frequencies that contribute significantly to ^{15}N-T_1 relaxation (*55*). Small $J_{eff}(0)$ and large $J(0.87\omega_H)$ values (the latter characteristics of very rapid picosecond to nanosecond motions) were observed for amides residing in the N- and C-terminal ends of the three proteins. These data are also very consistent with what is generally observed for very flexible disordered termini of proteins (*55*).

Interesting differences in $J_{eff}(0)$ and $J(0.87\omega_H)$ were observed for backbone amides residing within the helix D−turn−helix E domain of the three aporepressors (Table 1). As revealed by the ^{15}N−{^{1}H}-nOe trends, elevated values of $J(0.87\omega_H)$ were observed for these residues compared to those of backbone amides residing in the core helices of the proteins, indicating that backbone amides in the HTH regions of all three aporepressors are more flexible on a picosecond to nanosecond time scale than core amides. Residues that were not undergoing chemical

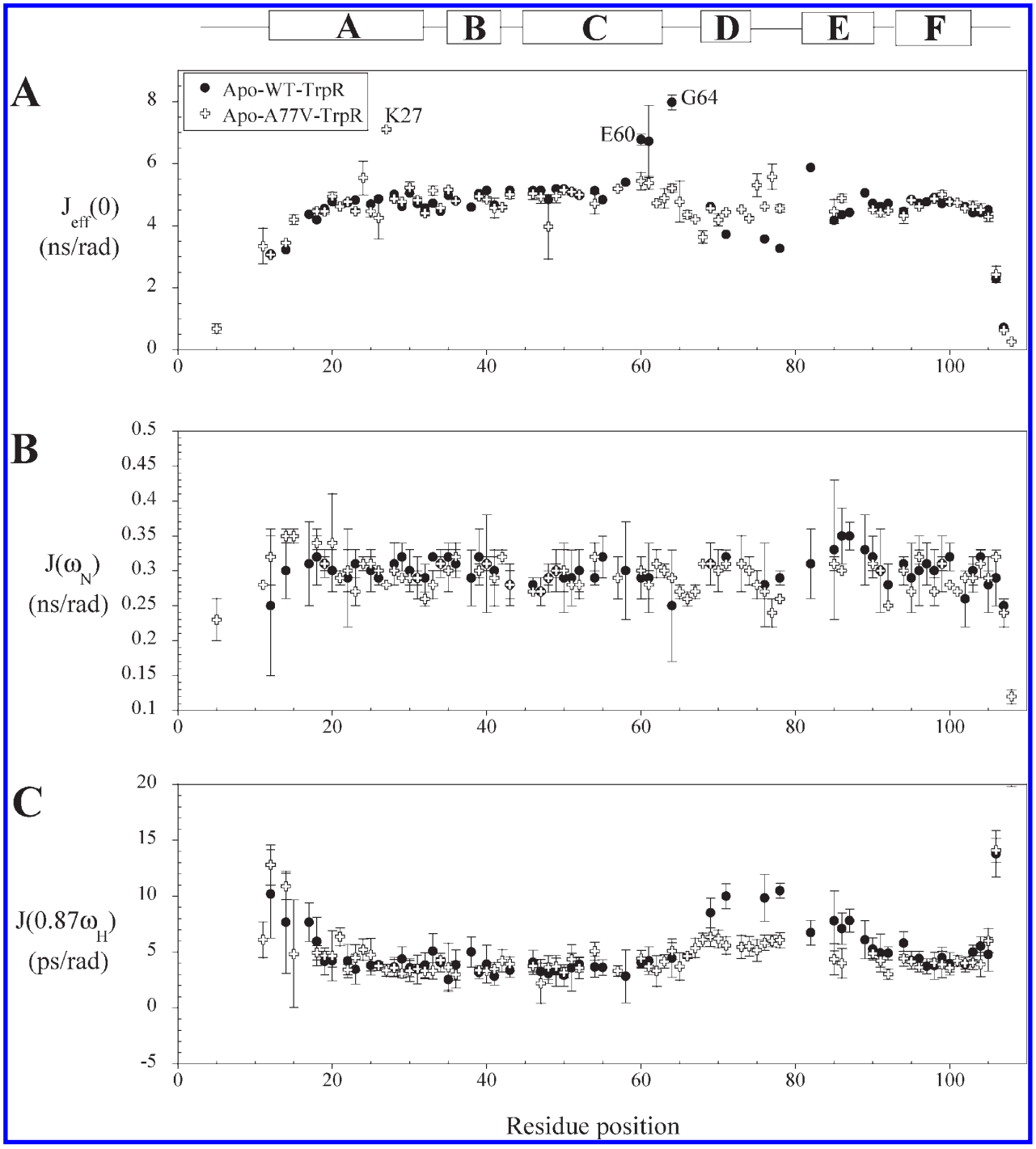

FIGURE 4: Comparison plots of reduced spectral density functions calculated for apo-WT-TrpR (filled circles) and apo-A77V-TrpR (open crosses): (A) $J_{eff}(0)$, (B) $J(\omega_N)$, and (C) $J(0.87\omega_H)$, with secondary structural elements depicted above the plots. Plotted error bars correspond to errors reported in Tables S6 and S7 of the Supporting Information. Residues with high $J_{eff}(0)$ values (suspected to include R_{exch}) from both proteins are labeled in panel A. Reduced $J(0.87\omega_H)$ trends for backbone amides in the helix D−turn−helix E region of apo-A77V-TrpR support the notion that the Ala to Val amino acid substitution at residue 77 decreases the overall picosecond to nanosecond motional flexibility of the HTH DNA-binding domain of the super-repressor.

exchange possessed $J_{eff}(0)$ values slightly lower than those measured for core amides (lower by ~0.5 ns/rad). Together, these data indicated that in all three aporepressors, the HTH domain has increased internal motions and is more flexible than core elements.

However, the patterns were not uniform across the D and E regions, and differential flexibility was again observed between the two regions (see Figures 3C and 4C and Table 1). For example, elevated $J(0.87\omega_H)$ values were measured for helix D amides of apo-WT-TrpR compared to $J(0.87\omega_H)$ values measured for the corresponding amides of apo-L75F-TrpR (Figure 3C) and apo-A77V-TrpR (Figure 4C), clearly indicating that the helix D region of apo-WT-TrpR is more flexible than helix D of apo-L75F-TrpR and that of apo-A77V-TrpR. The $J(0.87\omega_H)$ patterns are reversed for helix E amides of apo-L75F-TrpR, whereby $J(0.87\omega_H)$ trends are slightly higher than those calculated for helix E amides of apo-WT-TrpR (Figure 3C), indicating the E region is more flexible in apo-L75F-TrpR than in apo-WT-TrpR.

These data clearly show that the Leu to Phe mutation at residue 75 reduces the internal backbone motions of helix D

amides and enhances the picosecond to nanosecond motions of helix E amides. In contrast, the $J(0.87\omega_H)$ trends remain lower for helix E amides of apo-A77V-TrpR than for apo-WT-TrpR (Figure 4C), indicating that the Ala to Val substitution at residue 77 reduces picosecond to nanosecond internal motions throughout the entire helix D−turn−helix E domain of the super-repressor.

In the analysis of $J_{eff}(0)$ trends, several residues exhibited significantly large $J_{eff}(0)$ values, an indication that these residues not only are experiencing picosecond to nanosecond bond vector fluctuations but also undergo slower microsecond to millisecond chemical exchange motions. Elevated $J_{eff}(0)$ values were observed for residues E60 and G64 of apo-WT-TrpR and I82 of apo-L75F-TrpR, which suggest strong R_{exch} contributions to ^{15}N-T_2 relaxation. These results are consistent with ^{15}N-$T_{1\rho}$ measurements and calculations of ^{15}N-$T_{1\rho}$/^{15}N-T_2 ratios.

FastModelFree Analysis of ^{15}N NMR Relaxation Parameters. As mentioned, ^{15}N NMR relaxation parameters of all three aporepressors were also analyzed using the ModelFree approach of Palmer and colleagues (*59*, *60*, *64*). Details of such analysis are included as Supporting Information. Generalized order parameters computed as a result of FastModelFree analysis of the ^{15}N NMR relaxation data were consistent with the ^{15}N−{^{1}H}-nOe profiles observed for residues of the three aporepressors. However, interpretation of the data was limited because ^{15}N NMR relaxation data of many residues of interests could be fitted to only higher models of motion, indicating that these residues are undergoing motions too complex to be accurately parametrized by ModelFree. Despite this limitation, model selection according to the approach of Mandel et al. (*64*) did reveal noteworthy qualitative differences and subtleties in S^2 trends among the three apo-TrpR proteins as reported in the Supporting Information. Model fitting to models higher than model 1 or 2 could not provide quantitative information about the complex motions taking place in the HTH motif of the three proteins but did support findings that the dynamics profiles of backbone amides in this region are different for the three aporepressors. It also suggested that backbone motions in the HTH domains of apo-L75F-TrpR and apo-WT-TrpR are more complex than those of corresponding amides of apo-A77V-TrpR.

DISCUSSION

Molecular recognition is a fundamental element of protein function that often invokes both structural and dynamic changes upon formation of a complex between proteins and ligands (*38*, *68*, *69*). Structural and dynamic changes are particularly important for the function of DNA-binding proteins such as TrpR and selective protein binding to cognate DNA targets and to coeffector ligands. Native state protein flexibility is crucial for mediating effects such as allostery, a process requiring communication between distant sites or "action at a distance" (*70*−*72*). In the case of TrpR, dynamics plays a role as important as that of structure in modulating its DNA binding properties and biological function (*15*, *16*, *18*−*21*). Despite a wealth of information about the biochemical and biophysical properties of TrpR and of functionally altered TrpR variants, our understanding of the mechanisms by which internal flexibility modulates TrpR function is incomplete.

In these studies, ^{15}N NMR relaxation experiments were conducted to characterize picosecond to nanosecond dynamics of backbone amides of three different apo forms of TrpR, including apo-L75F-TrpR, apo-WT-TrpR, and apo-A77V-TrpR. The goal was to improve our understanding of how changes in backbone flexibility affect the L-Trp binding properties of the three different aporepressors. The two TrpR variants (apo-L75F-TrpR and apo-A77V-TrpR) were chosen in part because they are both results of a single conservative amino acid substitution in a solvent accessible loop (two residues apart in the protein sequence) yet exhibit opposite phenotypes in terms of L-Trp binding properties and differ considerably from apo-WT-TrpR. Apo-L75F-TrpR has been characterized as a ts mutant that at the permissive temperature of 42 °C allows cell growth on minimal medium containing 5-MT, while cells producing apo-WT-TrpR starve for L-Trp (*30*). In contrast to the weakened TrpR function of apo-L75F-TrpR, apo-A77V-TrpR displays enhanced TrpR function and increased repressor activity and regulation of the *trp* operator in vivo (*25*). For this reason, apo-A77V-TrpR has been designated a super-repressor (*73*−*75*).

In addition, the sites at which a conservative amino acid substitution has occurred in the two TrpR mutants (residue 75 and residue 77, respectively) and that manifest in very distinct L-Trp binding properties are separated in the TrpR sequence by only one residue and occur on a solvent accessible surface loop of the HTH domain. Despite their distinct phenotypes, both apo-L75F-TrpR and apo-A77V-TrpR possess very similar biophysical characteristics, including an ∼10% apparent increase in α-helical content compared to apo-WT-TrpR, and a small increase in chemical stability as implicated from CD and urea denaturation experiments (*24*, *29*, *30*), while all three proteins remain highly thermostable with almost identical T_m values of ∼90 °C (*30*).

These ^{15}N NMR relaxation studies have revealed that backbone amides located in the core helices of the three aporepressors are highly restricted in picosecond to nanosecond time scale motions, and that little difference in terms of backbone dynamics exists among the three proteins for core amides. Most of the dynamics differences observed among apo-L75F-TrpR, apo-WT-TrpR, and apo-A77V-TrpR are localized to the helix D−turn−helix E (HTH) DNA-binding domain of the three aporepressors. N−H bond vectors of helix D amides are found to be more flexible in apo-WT-TrpR than the corresponding amides of apo-L75F-TrpR and apo-A77V-TrpR. Reduced spectral density analysis of the three aporepressors has largely emphasized conclusions derived from examination of ^{15}N-T_1, ^{15}N-T_2, and ^{15}N−{^{1}H}-nOe patterns. The uniformity of ^{15}N-T_1 throughout the sequence is reflected in the uniformity of the $J(\omega_N)$ trends of the three aporepressors. These observations indicate that the TrpR variants do not differ globally from WT-TrpR and possess structural folds and diffusion properties very similar to those of the wild-type protein. However, analysis of the spectral density functions $J_{eff}(0)$ and $J(0.87\omega_H)$ reveals the presence of distinct dynamic subtleties specific to each aporepressor. $J_{eff}(0)$, which reports variations in slower time scale motions, including overall molecular tumbling and conformational switches, identifies regions near the C-terminal region of helix C of apo-WT-TrpR to be undergoing slower microsecond to millisecond conformational exchange, which appears to be absent in the TrpR mutants. In addition, low $J_{eff}(0)$ and high $J(0.87\omega_H)$ values for backbone amides in the HTH DNA-binding domain of the aporepressors confirm that helices D and E are highly flexible on fast picosecond to nanosecond time scales with "flexibility hubs" located at different sites within the helix D−turn−helix E region of each apo-TrpR protein. Altogether, these results are consistent with previous observations of additional

$^{1}H-^{1}H$ nOe connectivities for apo-L75F-TrpR compared to apo-WT-TrpR, which suggested that helix D in the L75F-TrpR protein was more ordered (and in all likelihood less flexible) than its counterpart in wild-type TrpR (*34*).

Noticeable differences in picosecond to nanosecond dynamics were also observed among the three aporepressors for N−H bond vectors located within helix E. Helix E amides were found to be motionally more restricted in apo-WT-TrpR than corresponding helix E amides of apo-L75F-TrpR. The ^{15}N NMR relaxation parameters and spectral density data analysis indicated that helix E amides of apo-L75F-TrpR have a significant increase in picosecond to nanosecond motional flexibility compared to corresponding amides of apo-WT-TrpR. $^{15}N-\{^{1}H\}$-nOe data collected at 37 °C (nonpermissive temperature of the apo-L75F-TrpR ts mutant) (data not shown) displayed trends identical to those observed at 45 °C (a temperature 3 °C higher than the permissive temperature of the apo-L75F-TrpR ts mutant, 42 °C), enabling us to conclude that the flexibility of helix E of apo-L75F-TrpR is not altered by a switch from the permissive to the nonpermissive temperature. Similarly, no changes in the backbone dynamics of helix D amides were observed at the permissive temperature (37 °C) compared to their dynamics profile observed at 45 °C. These observations lead us to conclude that the ts phenotype of apo-L75F-TrpR is not manifested by a change in picosecond to nanosecond backbone amide dynamics of the protein's DNA-binding domain at the two different temperatures.

Helix E holds special significance to TrpR, as it serves as the recognition helix that "identifies" operator DNA sites and binds with the major groove of the DNA double helix in a "head-on" fashion. In addition, of the five residues that hold the L-Trp molecule in its place in the L-Trp binding site of each protomer of the TrpR dimer (R54, T81, R84, L41′, and T44′), two (T81 and R84) are located on the N-terminus of helix E. From our comparison of $^{15}N-\{^{1}H\}$-nOe data recorded at 45 °C versus 37 °C, we infer that the picosecond to nanosecond dynamics profile of apo-L75F-TrpR stays reasonably consistent from 45 to 42 °C (permissive temperature). With this in mind, we propose that the disorder-to-order energy barrier may be too high in the ts TrpR mutant to be overcome by L-Trp binding at permissive temperatures. The failure of apo-L75F-TrpR to generate a well-ordered helix E that may form appropriate contacts in the major groove could provide a rationale for the L75F-TrpR mutant's phenotype.

We rationalize that the apparent increase in α-helicity observed in apo-L75F-TrpR is due to the formation of a more ordered, less flexible, helix D as a result of the leucine to phenylalanine amino acid substitution at residue 75. Formation of a preordered helix D in apo-L75F-TrpR may create an additional energy barrier precluding the formation of a well-ordered helix E upon L-Trp binding. In other words, we postulate that the decrease in flexibility and preordering (although this helix remains considerably more dynamic than core helices) of helix D provides a small additional energy barrier to the sequential ordering of helix E upon L-Trp corepressor binding. In the case of apo-WT-TrpR, helix E is the first to form into a well-defined α-helix upon formation of holo-WT-TrpR (*17*−*20*), which is followed by formation of a well-ordered helix D upon formation of a complex of holo-WT-TrpR with cognate DNA (*21*). In apo-L75F-TrpR, the preordering of helix D [as inferred from the dynamics studies here and the observation of additional interproton nOes in its structure determination (*34*)] may interfere with the ordering of helix E upon holo-L75F-TrpR formation. The decreased flexibility of helix D amides could be a contributing factor to the 10-fold weaker L-Trp binding affinity of apo-L75F-TrpR compared to that of apo-WT-TrpR (*30*).

Consistent with the work of Jardetzky and co-workers (*18*), we find that backbone amides located within the helix D−turn−helix E domain of apo-A77V-TrpR are more restricted in terms of picosecond to nanosecond motions than their counterparts in apo-WT-TrpR. Helix E amides of apo-A77V-TrpR are also less flexible than the corresponding amides of apo-L75F-TrpR. The overall decrease in flexibility of the helix D−turn−helix E domain of apo-A77V-TrpR [i.e., decrease in internal motions on a wide range of time scales as observed in this work and that of Jardetzky and co-workers (*17*, *73*)] suggests that the ability of apo-A77V-TrpR to repress gene expression at low L-Trp concentrations may be due to a preordering of the protein's DNA-binding domain. The reduced dynamics of apo-A77V-TrpR would thus mimic more closely the molecular characteristics of holo-WT-TrpR.

Previous studies showed that the ability of apo-A77V-TrpR to discriminate between operator and nonoperator DNA is impaired compared to that of WT-TrpR (*76*). Our studies suggest that the reduced flexibility of both helix D and helix E amides of apo-A77V-TrpR may be at the source of this impaired molecular recognition function.

The integral interdependence of structure, dynamics, and function is well-established for TrpR, especially with respect to the importance of disorder-to-order transitions observed for structural elements within the helix D−turn−helix E domain upon L-Trp and DNA binding (*20*, *25*). The lower $^{15}N-\{^{1}H\}$-nOes and higher $J(0.87\omega_H)$ values observed for backbone amides of helix D of apo-WT-TrpR support the notion that sequential ordering of helices E and D upon L-Trp and DNA binding is essential for proper TrpR function (*21*).

The adaptability of helix E for DNA binding is related to the ability (and indeed the requirement, dictated by the DNA sequence) of TrpR to bind as a single dimer at the TrpR operator, but as tandem dimers at the other operators of the regulon. In the absence of L-Trp, TrpR cannot discriminate between operator and nonoperator DNAs (binding affinities are equal). However, in the presence of L-Trp, operator DNA is bound ~200-fold more strongly but nonoperator DNA is bound no more strongly than in the absence of L-Trp (*77*). Thus, it is clear that L-Trp enhances both the affinity and specificity of TrpR−DNA interactions. Both apo-L75F-TrpR and apo-A77V-TrpR exhibit altered L-Trp binding properties that originate from differences in dynamics between the TrpR mutants and WT-TrpR. Our studies suggest that modified dynamics should have a major impact on the DNA binding and binding specificity (i.e., the ability to discriminate between operator and nonoperator DNA) properties of apo-L75F-TrpR and apo-A77V-TrpR.

In summary, the ^{15}N NMR relaxation studies presented herein have revealed small but significant variations in ^{15}N backbone amide dynamics occurring on the picosecond to nanosecond time scale among the three TrpR aporepressors whose L-Trp corepressor binding properties differ remarkably. We find that helix D amides are less flexible in apo-L75F-TrpR than their counterparts in apo-WT-TrpR. The situation is reversed for helix E amides, which exhibit a greater degree of flexibility in the L75F-TrpR mutant than the corresponding amides in WT-TrpR. These data suggest that this differential flexibility, although subtle, is an important contributor to the 10-fold lower L-Trp corepressor

binding affinity of L75F-TrpR. The fast picosecond to nanosecond internal motions occurring in helix E of apo-L75F-TrpR could justify a stronger energy requirement to stabilize L-Trp binding in the L-Trp binding pocket of the ts TrpR mutant, which would translate into a lower L-Trp binding affinity as observed for this TrpR mutant.

In contrast to apo-L75F-TrpR, ^{15}N backbone amide dynamics studies of apo-A77V-TrpR do not reveal such significant differences between the dynamics profiles of amides located in the core helices versus those located in the helix D−turn−helix E domain of this TrpR super-repressor. Amides in the HTH DNA-binding domain of A77V-TrpR are as motionally restricted as core amides of the protein.

This study reinforces the importance of the intrinsic dynamic nature of helix D and the turns flanking the HTH domain of all three aporepressors. We therefore conclude that TrpR can achieve proper function only if it is comprised of an optimal amount of flexibility (encompassing motions on a wide range of time scales), and minor dynamics perturbations especially in the helix D−turn−helix E DNA-binding domain of the repressor can prove to be detrimental to the protein's function.

ACKNOWLEDGMENT

The NMR experiments were conducted at Montana State University on a Bruker DRX600 NMR spectrometer purchased in part with funds from the National Institutes of Health Shared Instrumentation Grant Program (Grant 1-S10RR13878-01) and the NSF-EPSCOR program for the State of Montana. We acknowledge the Montana State University Research Experience for Undergraduate (REU) program (National Science Foundation Grant NSF-0852043), which supported REU students Lucas Nebert, Melinda Park, and Stacey Moates to conduct research in our laboratory. We thank Stacey Moates and Melinda Park for help with expression and purification of ^{15}N-labeled and ^{15}N- and ^{13}C-labeled apo-A77V-TrpR during their REU summer internship at Montana State University.

SUPPORTING INFORMATION AVAILABLE

Supplemental tables (S1−S10) and a detailed text description of the FastModelFree analysis of measured ^{15}N NMR relaxation parameters. This material is available free of charge via the Internet at http://pubs.acs.org.

REFERENCES

1. Joachimiak, A., Kelley, R. L., Gunsalus, R. P., Yanofsky, C., and Sigler, P. B. (1983) Purification and characterization of trp aporepressor. *Proc. Natl. Acad. Sci. U.S.A. 80*, 668–672.
2. Sigler, P. B. (1992) Transcriptional Regulation, Cold Spring Harbor Laboratory Press, Plainview, NY.
3. Klig, L. S., Carey, J., and Janofsky, C. (1988) trp repressor interactions with the trp aroH and trpR operators: Comparison of repressor binding in vitro and repression in vivo. *J. Mol. Biol. 202*, 769–777.
4. Gunsalus, R. P., and Yanofsky, C. (1980) Nucleotide sequence and expression of *Escherichia coli* trpR, the structural gene for the trp aporepressor. *Proc. Natl. Acad. Sci. U.S.A. 77*, 7117–7121.
5. Zurawski, G., Gunsalus, R. P., Brown, K. D., and Yanofsky, C. (1981) Structure and regulation of *aroH*, the structural gene for the tryptophan-repressible 3-deoxy-D-arabino-heptulosonic acid-7-phosphate synthetase of *Escherichia coli*. *J. Mol. Biol. 145*, 47–57.
6. Sarsero, J. P., Wookey, P. J., and Pittard, A. J. (1991) Regulation and expression of *Escherichia coli* K-12 mtr gene by TyrR and trp repressor. *J. Bacteriol. 173*, 4133–4143.
7. Carey, J., Lewis, D. E., Lavoie, T. A., and Yang, J. (1991) How does trp repressor bind to its operator? *J. Biol. Chem. 266*, 24509–24513.
8. Lavoie, T. A., and Carey, J. (1994) Adaptability and specificity in DNA binding by trp repressor. *Nucleic Acid Mol. Biol. 8*, 185–196.
9. Marmorstein, R. Q., Joachimiak, A., Sprinzl, M., and Sigler, P. B. (1987) The structural basis for the interaction between L-tryptophan and the *Escherichia coli* trp aporepressor. *J. Biol. Chem. 262*, 4922–4927.
10. Luisi, B. F., and Sigler, P. B. (1990) The stereochemistry and biochemistry of the trp repressor-operator complex. *Biochim. Biophys. Acta 1048*, 113–126.
11. Yang, J., Gunasekera, A., Lavoie, T. A., Jin, L., Lewis, D. E. A., and Carey, J. (1996) In vivo and in vitro studies of TrpR-DNA interactions. *J. Mol. Biol. 258*, 37–52.
12. Schevitz, R. W., Otwinowski, Z., Joachimiak, A., Lawson, C. L., and Sigler, P. B. (1985) The three-dimensional structure of trp repressor. *Nature 317*, 782–786.
13. Zhang, R. G., Joachimiak, A., Lawson, C. L., Schevitz, R. W., Otwinowski, Z., and Sigler, P. B. (1987) The crystal structure of trp aporepressor at 1.8 Å shows how binding tryptophan enhances DNA affinity. *Nature 327*, 591–597.
14. Otwinowski, Z., Schevitz, R. W., Zhang, R. G., Lawson, C. L., Joachimiak, A., Marmorstein, R. Q., Luisi, B. F., and Sigler, P. B. (1988) Crystal structure of trp repressor/operator complex at atomic resolution. *Nature 335*, 321–329.
15. Arrowsmith, C., Pachter, R., Altman, R., and Jardetzky, O. (1991) The solution structures of *Escherichia coli* trp repressor and trp aporepressor at an intermediate resolution. *Eur. J. Biochem. 202*, 53–66.
16. Zhao, D., Arrowsmith, C. H., Jia, X., and Jardetzky, O. (1993) Refined solution structures of the *Escherichia coli* trp holo- and aporepressor. *J. Mol. Biol. 229*, 735–746.
17. Finucane, M. D., and Jardetzky, O. (1995) Mechanism of hydrogen-deuterium exchange in trp repressor studied by ^{1}H-^{15}N NMR. *J. Mol. Biol. 253*, 576–589.
18. Gryk, M. R., Finucane, M. D., Zheng, Z., and Jardetzky, O. (1995) Solution dynamics of the trp repressor: A study of amide proton exchange by T1 relaxation. *J. Mol. Biol. 246*, 618–627.
19. Zheng, Z., Czaplicki, J., and Jardetzky, O. (1995) Backbone dynamics of trp repressor studied by ^{15}N NMR relaxation. *Biochemistry 34*, 5212–5223.
20. Czaplicki, J., Arrowsmith, C., and Jardetzky, O. (1991) Segmental differences in the stability of the trp repressor peptide backbone. *J. Biomol. NMR 1*, 349–361.
21. Zhang, H., Zhao, D., Revington, M., Lee, W., Jia, X., Arrowsmith, C., and Jardetzky, O. (1994) The solution structures of the trp repressor-operator DNA complex. *J. Mol. Biol. 238*, 592–614.
22. Bae, S. J., Chou, W. Y., Matthews, K. S., and Sturtevant, J. M. (1988) Tryptophan repressor of *E. coli* shows unusual thermal stability. *Proc. Natl. Acad. Sci. U.S.A. 85*, 6731–6732.
23. Gittelman, M. S., and Matthews, C. R. (1990) Folding and stability of trp aporepressor from *Escherichia coli*. *Biochemistry 29*, 7011–7020.
24. Schmitt, T. H., Zheng, Z., and Jardetzky, O. (1995) Dynamics of tryptophan binding to *Escherichia coli* Trp repressor wild type and AV77 mutant: An NMR study. *Biochemistry 34*, 13183–13189.
25. Gryk, M. R., Jardetzky, O., Klig, L. S., and Yanofsky, C. (1996) Flexibility of DNA binding domain of trp repressor required for recognition of different operator sequences. *Protein Sci. 5*, 1195–1197.
26. Chou, W. Y., and Matthews, K. S. (1989) Serine to cysteine mutations in trp repressor protein alter tryptophan and operator binding. *J. Biol. Chem. 264*, 18314–18319.
27. Bass, S., Sorrells, V., and Youderian, P. (1988) Mutant Trp repressors with new DNA-binding specificities. *Science 242*, 240–245.
28. Kelley, R. L., and Yanofsky, C. (1985) Mutational studies with the trp repressor of *Escherichia coli* support the helix-turn-helix model of repressor recognition of operator DNA. *Proc. Natl. Acad. Sci. U.S.A. 82*, 483–487.
29. Gryk, M. R., and Jardetzky, O. (1996) AV77 hinge mutation stabilizes the helix-turn-helix domain of trp repressor. *J. Mol. Biol. 255*, 204–214.
30. Jin, L., Fukayama, J. W., Pelczer, I., and Carey, J. (1999) Long-range effects on dynamics in a temperature-sensitive mutant of trp repressor. *J. Mol. Biol. 285*, 361–378.
31. Marmorstein, R. Q., and Sigler, P. B. (1989) Stereochemical effects of L-tryptophan and its analogues on trp repressor's affinity for operator-DNA. *J. Biol. Chem. 264*, 9149–9154.
32. Lawson, C. L. (1996) Structural consequences of two methyl additions in the *E. coli* trp repressor L-tryptophan binding pocket. In Proceedings of the 9th Convention in Biomolecular Stereodynamics (Sarma, R. H., and Sarma, M. H., Ed.) pp 83−90, Adenine Press, Schenectady, NY.
33. Bennett, G. N., and Yanofsky, C. (1978) Sequence analysis of operator constitutive mutants of the tryptophan operon of *Escherichia coli*. *J. Mol. Biol. 121*, 179–192.

34. Tyler, R., Pelczer, I., Carey, J., and Copie, V. (2002) Three-dimensional solution NMR structure of Apo-L75F-TrpR, a temperature-sensitive mutant of the tryptophan repressor protein. *Biochemistry 41*, 11954–11962.
35. Kay, L. E. (1998) Protein dynamics from NMR. *Biochem. Cell Biol. 76*, 145–152.
36. Palmer, A. G., Kroenke, C. D., and Loria, J. P. (2001) NMR methods for quantifying microsecond-to-millisecond motions in biological macromolecules. *Methods Enzymol. 339*, 204–238.
37. Palmer, A. G. (2001) NMR probes of molecular dynamics: Overview and comparison with other techniques. *Annu. Rev. Biophys. Biomol. Struct. 30*, 129–155.
38. Wand, J. A. (2001) Dynamic activation of protein function: A view emerging from NMR spectroscopy. *Nat. Struct. Biol. 8*, 926–931.
39. Lee, A. L., Flynn, P. F., and Wand, A. J. (1999) Comparison of H-2 and C-13 NMR relaxation techniques for the study of protein methyl group dynamics in solution. *J. Am. Chem. Soc. 121*, 2891–2902.
40. Paluh, J. L., and Yanofsky, C. (1986) High level production and rapid purification of the *E. coli* trp repressor. *Nucleic Acids Res. 14*, 7851–7860.
41. Bodenhausen, G., and Ruben, D. J. (1980) Natural Abundance Nitrogen-15 NMR by Enhanced Heteronuclear Spectroscopy. *Chem. Phys. Lett. 69*, 185–189.
42. Shaka, A. J., Keeler, J., and Freeman, R. (1983) Evaluation of A New Broad-Band Decoupling Sequence: Waltz-16. *J. Magn. Reson. 53*, 313–340.
43. Grzesiek, S., and Bax, A. (1992) Correlating Backbone Amide and Side-Chain Resonances in Larger Proteins by Multiple Relayed Triple Resonance NMR. *J. Am. Chem. Soc. 114*, 6291–6293.
44. Kay, L. E., Ikura, M., Tschudin, R., and Bax, A. (1990) Three-dimensional triple-resonance NMR spectroscopy of isotopically enriched proteins. *J. Magn. Reson. 89*, 496–514.
45. Wittekind, M., and Mueller, L. (1993) HNCACB, a High-Sensitivity 3D NMR Experiment to Correlate Amide-Proton and Nitrogen Resonances with the α- and β-Carbon Resonances in Proteins. *J. Magn. Reson., Ser. B 101*, 201–205.
46. Delaglio, F., Grzesiek, S., Vuister, G. W., Zhu, G., Pfeifer, J., and Bax, A. (1995) NMRPipe: A Multidimensional Spectral Processing System Based on Unix Pipes. *J. Biomol. NMR 6*, 277–293.
47. Goddard, T. D., and Kneller, D. G. (2002) SPARKY 3, University of California, San Francisco.
48. Barbato, G., Ikura, M., Kay, L. E., Pastor, R. W., and Bax, A. (1992) Backbone dynamics of calmodulin studied by ^{15}N relaxation using inverse detected two-dimensional NMR spectroscopy: The central helix is flexible. *Biochemistry 31*, 5269–5278.
49. Kay, L. E., Torchia, D. A., and Bax, A. (1989) Backbone dynamics of proteins as studied by ^{15}N inverse detected heteronuclear NMR spectroscopy: Application to staphylococcal nuclease. *Biochemistry 28*, 8972–8979.
50. Grzesiek, S., and Bax, A. (1993) The Importance of Not Saturating H_2O in Protein NMR. *J. Am. Chem. Soc. 115*, 12593–12594.
51. Carr, H. Y., and Purcell, E. M. (1954) Effects of Diffusion on Free Precession in Nuclear Magnetic Resonance Experiments. *Phys. Rev. 94*, 630.
52. Meiboom, S., and Gill, D. (1958) Modified Spin-Echo Method for Measuring Nuclear Relaxation Times. *Rev. Sci. Instrum. 29*, 688–691.
53. Palmer, A. G., Rance, M., and Wright, P. E. (1991) Intramolecular motions of a zinc finger DNA-binding domain from Xfin characterized by proton-detected natural abundance ^{13}C heteronuclear NMR spectroscopy. *J. Am. Chem. Soc. 113*, 4371–4380.
54. Nicholson, L. K., Kay, L. E., Baldisseri, D. M., Arango, J., Young, P. E., Bax, A., and Torchia, D. A. (1992) Dynamics of methyl groups in proteins as studied by proton-detected ^{13}C NMR spectroscopy. Application to the leucine residues of staphylococcal nuclease. *Biochemistry 31*, 5253–5263.
55. Bracken, C., Carr, P. A., Cavanagh, J., and Palmer, A. G., III (1999) Temperature dependence of intramolecular dynamics of the basic leucine zipper of GCN4: Implications for the entropy of association with DNA. *J. Mol. Biol. 285*, 2133–2146.
56. Bhattacharya, N., Yi, M., Zhou, H.-X., and Logan, T. M. (2007) Backbone dynamics in an intramolecular prolylpeptide-SH3 complex from the diphteria toxin repressor, DtxR. *J. Mol. Biol. 374*, 977–992.
57. Farrow, N. A., Zhang, O. W., Szabo, A., Torchia, D. A., and Kay, L. E. (1995) Spectral Density-Function Mapping Using N-15 Relaxation Data Exclusively. *J. Biomol. NMR 6*, 153–162.
58. Blumenschein, T. M. A., Stone, D. B., Fletterick, R. J., Mendelson, R. A., and Sykes, B. A. (2006) Dynamics of the C-terminal region of TnI in the troponin complex in solution. *Biophys. J. 90*, 2436–2444.
59. Cole, R., and Loria, J. P. (2003) FAST-model free: A program for rapid automated analysis of solution NMR spin-relaxation data. *J. Biomol. NMR 26*, 203–213.
60. Palmer, A. (1998) ModelFree, version 4.0. http://cpmcnet.columbia.edu/dept/gsas/biochem/labs/palmer.
61. Lipari, G., and Szabo, A. (1982) Model-Free Approach to the Interpretation of Nuclear Magnetic-Resonance Relaxation in Macromolecules. 1. Theory and Range of Validity. *J. Am. Chem. Soc. 104*, 4546–4559.
62. Lipari, G., and Szabo, A. (1982) Model-Free Approach to the Interpretation of Nuclear Magnetic-Resonance Relaxation in Macromolecules. 2. Analysis of Experimental Results. *J. Am. Chem. Soc. 104*, 4559–4570.
63. Pawley, N. H., Wang, C., Koide, S., and Nicholson, L. K. (2001) An improved method for distinguishing between anisotropic tumbling and chemical exchange in analysis of ^{15}N relaxation parameters. *J. Biomol. NMR 20*, 149–165.
64. Mandel, A. M., Akke, M., and Palmer, A. G. (1995) Backbone dynamics of *Escherichia coli* ribonuclease HI: Correlations with structure and function in an active enzyme. *J. Mol. Biol. 246*, 144–163.
65. Peng, J. W., and Wagner, G. (1992) Mapping of the Spectral Densities of N-H Bond Motions in Eglin-C Using Heteronuclear Relaxation Experiments. *Biochemistry 31*, 8571–8586.
66. Peng, J. W., and Wagner, G. (1992) Mapping of Spectral Density-Functions Using Heteronuclear NMR Relaxation Measurements. *J. Magn. Reson. 98*, 308–332.
67. Farrow, N. A., Muhandiram, R., Singer, A. U., Pascal, S. M., Kay, C. M., Gish, G., Shoelson, S. E., Pawson, T., Forman-Kay, J. D., and Kay, L. E. (1994) Backbone dynamics of a free and phosphopeptide-complexed Src homology 2 domain studied by ^{15}N NMR relaxation. *Biochemistry 33*, 5984–6003.
68. Formaneck, M. S., Ma, L., and Cui, Q. (2006) Reconciling the "old" and "new" view of protein allostery: A molecular simulation study of chemotaxis Y protein (chey). *Proteins: Struct., Funct., Bioinf. 63*, 846–867.
69. Karplus, M., and Kuryan, J. (2005) Molecular dynamics and protein function. *Proc. Natl. Acad. Sci. U.S.A. 102*, 6679–6685.
70. Kern, D., and Zuiderweg, E. R. P. (2003) The role of dynamics in allosteric regulation. *Curr. Opin. Struct. Biol. 13*, 748–757.
71. Popovych, N., Sun, S., Ebright, R. H., and Kalodimos, C. G. (2006) Dynamically driven protein allostery. *Nat. Struct. Biol. 13*, 831–838.
72. Clarkson, M. W., Gilmore, S. A., Edgell, M. H., and Lee, A. L. (2006) Dynamic coupling and allosteric behavior in a nonallosteric protein. *Biochemistry 45*, 7693–7699.
73. Finucane, M. D., and Jardetzky, O. (2003) Surface plasmon resonance studies of wild-type and AV77 tryptophan repressor resolve ambiguities in super-repressor activity. *Protein Sci. 12*, 1613–1620.
74. Reedstrom, R. J., and Royer, C. A. (1995) Evidence for coupling of folding and function in trp repressor: Physical characterization of the superrepressor mutant AV77. *J. Mol. Biol. 253*, 266–276.
75. Reedstrom, R. J., Martin, K. S., Vangala, S., Mahoney, S., Wilker, E. W., and Royer, C. A. (1996) Characterization of charge change super-repressor mutants of trp repressor: Effects on oligomerization conformation, ligation and stability. *J. Mol. Biol. 264*, 32–45.
76. Grillo, A. O., and Royer, C. A. (2000) The basis for the super-repressor phenotypes of the AV77 and EK18 mutants of trp repressor. *J. Mol. Biol. 295*, 17–28.
77. Carey, J. (1988) Gel Retardation at Low pH Resolves trp Repressor-DNA Complexes for Quantitative Study. *Proc. Natl. Acad. Sci. U.S.A. 85*, 975–979.